ACS NANO
Cite This: ACS Nano XXXX, XXX, XXX−XXX
www.acsnano.org

ARTICLE

Wide Angle Dynamically Tunable Enhanced Infrared Absorption on Large-Area Nanopatterned Graphene

Alireza Safaei,[†,‡,‡] Sayan Chandra,[‡,‡] Michael N. Leuenberger,[†,‡,§] and Debashis Chanda*[,†,‡,§]

[†]Department of Physics, University of Central Florida, Orlando, Florida 32816, United States
[‡]NanoScience Technology Center, University of Central Florida, Orlando, Florida 32816, United States
[§]CREOL, The College of Optics and Photonics, University of Central Florida, Orlando, Florida 32816, United States

Supporting Information

ABSTRACT: Enhancing light-matter interaction by exciting Dirac plasmons on nanopatterned monolayer graphene is an efficient route to achieve high infrared absorption. Here, we designed and fabricated hexagonal planar arrays of nanoholes and nanodisks with and without optical cavity to excite Dirac plasmons on patterned graphene and investigate the role of plasmon lifetime, extinction cross-section, incident light polarization, angle of incident light, and pattern dimensions on the light-absorption spectra. By incorporating a high-k Al_2O_3 layer as the gate dielectric for dynamic electrostatic tuning of the Fermi level, we demonstrate peak absorptions of 60% and 90% for the nanohole and nanodisk patterns, respectively, in the atmospheric transparent 8−12 μm infrared imaging band with high spectral tunability. Finally, we theoretically and experimentally demonstrate angular dependence of both s- and p-polarized light absorption in monolayer graphene. Our results showcase the practical usability of low carrier mobility CVD-grown graphene for wide angle infrared absorption, which is suitable for next-generation optoelectronic devices such as photodetectors, optical switches, modulators, *etc.*

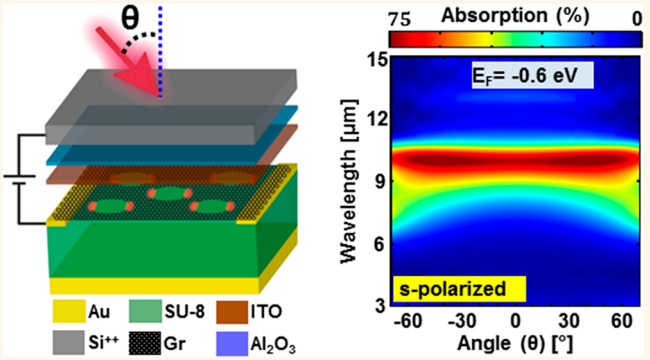

KEYWORDS: *graphene, light-matter interaction, localized Dirac plasmon, optical cavity, electrostatic tunability, mid-infrared spectral domain, plasmon lifetime*

Graphene is one of the more widely studied two-dimensional materials due to its special electrical and optical properties. Various promising strategies and ideas are being proposed for optical, electrical, and mechanical devices based on monolayer graphene by taking advantage of its properties, such as high carrier mobility,[1−6] fast carrier relaxation time, and electrostatic tunability in the devices such as transistors,[7] photodetectors,[8,9] optical switches,[10] nano-lasers,[11] and chemical sensors.[12−14] Compared to other two-dimensional materials, large-scale monolayer graphene can be grown easily using the chemical vapor deposition (CVD) technique, which makes real-world graphene-based optoelectronic devices viable even with lower carrier mobility compared to the mechanically exfoliated flakes. However, a major bottleneck is the low light−matter interaction in graphene that needs to be enhanced. Graphene is an ultrathin semimetal with a Dirac point in the band structure where the conduction and valence bands cross, leading to a constant light absorption (~2.3%) in the visible regime[15] and low absorption (<3%) in the mid-IR wavelength ranges.[16] Different strategies have been pursued to increase the interaction of the incident light with monolayer graphene while preserving its inherent properties such as high carrier mobility and fast relaxation time. To establish the feasibility of graphene-based infrared absorbers and detectors, three critical aspects need to be considered: (i) dependence of absorption to the angle of incidence, (ii) spectral tunability and selectivity for wide band operation, and (iii) polarization dependence. Ideally, polarization and angle-independent absorption are desirable properties of an absorber. Coupling the near field of a metallic metasurface or photonic crystal to graphene[10,17−21] is an indirect solution to increase the light−graphene interaction. However, in this scheme, the majority of incident light is dissipated as resistive ohmic loss in the metal, defeating the purpose. Additionally, owing to asymmetric metasurface designs, most of the absorbers reported to date are sensitive to the polarization of incident

Received: August 29, 2018
Accepted: December 7, 2018
Published: December 7, 2018

DOI: 10.1021/acsnano.8b06601
ACS Nano XXXX, XXX, XXX−XXX

light and exhibit limited spectral tunability.[22−24] In another approach, coupling a pristine[25] and nanopatterned[26−28] monolayer graphene to an optical cavity has been implemented to enhance absorption. Although these recent works have experimentally demonstrated the enhancement of absorption for normal incident light,[22−24,28,29] little is known about their absorption at higher angles of incidence, incident polarization, or the effect of pattern edge states in combination with doping level.

In the infrared domain, exciting Dirac plasmons[30] on nanopatterned graphene has been adopted as a route to couple and concentrate the incident light directly on the surface, thereby enhancing the infrared absorption.[27,29,31−33] Depending on the nanopattern design, the Dirac plasmons on graphene can be propagating surface plasmon polaritons (SPP) or localized surface plasmons (LSPs) modes. Plasmons are qualitatively characterized by their lifetimes. Longer lifetime results in stronger electric field confinement, which manifests as higher and sharper absorption (lower FWHM) in the spectral response. It has been reported that nanopatterning of graphene introduces graphene edges, which play a vital role in modifying the light absorption spectrum. Edge scattering effects and radiative and nonradiative decay arising from Landau damping through interband and intraband transitions contribute collectively to increase the decay rates of the plasmonic excitations.[28,30,34−38] Therefore, the fundamental question that arises is how critical is the role of graphene edge on the localized surface plasmon (LSP) excitation, decay rate, and overall absorption behavior of patterned graphene? Here, in order to investigate these aspects, we identified complementary nanostructures, *i.e.*, nanoholes and nanodisks, such that the qualitative natures of the edges are similar. A direct comparison of these complementary structures elucidates the differences in the plasmonic excitations, the degree of electrostatic spectral tunability, and polarization dependences as a function of incident angle. We adopt a combinatorial investigation using theory and experiment to gain insight into the underlying physical phenomena. Based on this, we demonstrate the effect of graphene nanopatterning and the edges on the plasmon lifetime and the light absorption. The maximum achieved light absorption is experimentally measured to be 90% (60%) for the cavity-coupled graphene nanodisk (nanohole) array for the specified geometry and E_F = −1 eV. This enhanced absorption is independent of the light polarization. An ideal strategy to enhance the light−graphene interaction should be independent of the angle of the incident light (θ_i). Here, we measure the dependence of the light absorption as a function of θ_i for s- and p-polarized light, which shows excellent agreement with the simulated results. The wide-angle absorption of unpolarized light by the patterned nanohole/nanodisk graphene devices are almost independent of the angle of incidence for $\theta_i < 50°$.

RESULTS AND DISCUSSION

Plasmonic Resonances in the Complementary Arrays. The architecture of the proposed graphene absorber is illustrated in Figure 1a. Pristine graphene grown on copper foil by the CVD method was transferred to the Si^{2+} (100 μm)/Al_2O_3 (15 nm)/ITO (10 nm) substrate. A layer of Ti/Au (5 nm/50 nm) was deposited on the transferred graphene to accumulate the electrical charge over the graphene sheet effectively. The hole/disk diameter (D) and period (P) were varied to tune the LSPR at a desired wavelength whereby the

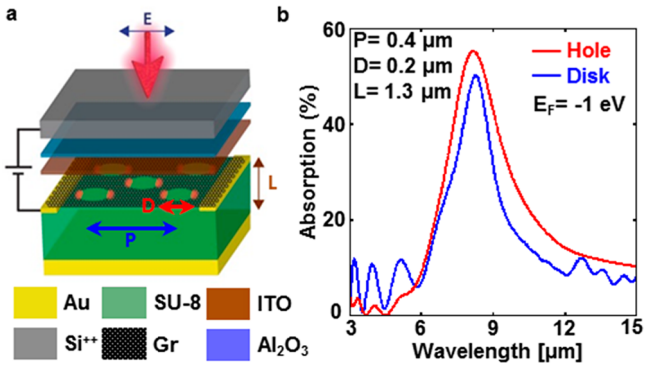

Figure 1. (a) Schematic of the optical cavity-coupled patterned graphene. The top layers are depicted separately to be distinguishable. (b) Light absorption spectra of the optical cavity-coupled graphene hole (red) and disk (blue) arrays with P = 400 nm, D = 200 nm, L = 1300 nm, and E_F = −1 eV.

cavity length was chosen to satisfy the quarter wavelength condition $L = m\lambda/4n_{eff}$.[39−41] Under these conditions, constructive interference of the incident and reflected electric fields on graphene sheet intensifies the LSPs and enhances the light−matter interaction, as shown in Figure S1 and in our previous work.[28] Here, L is the cavity thickness, n_{eff} is the effective refractive index of the optical cavity spacer, m is the mth order of the cavity mode, and λ is the light wavelength. The optical response of the designed graphene absorber was simulated by finite-difference time-domain (FDTD) approach. In these simulations, the mobility of graphene was chosen to be a modest 500 $cm^2/V{\cdot}s$ (scattering rate Γ = 0.02 eV) to closely resemble the experimentally measured mobility (see the SI), and the optical constants of graphene corresponding to different Fermi energies were calculated using the Drude model.[2,28]

The total light absorption spectra of the optical cavity-coupled nanopatterned graphene are different for the complementary graphene nanodisk and nanohole arrays with P = 400 nm, D = 200 nm, and L = 1.3 μm, as shown in Figure 1b, such that the peak bandwidth of the graphene nanodisk is smaller than that of its complementary graphene nanohole array. Interestingly, while the plasmon lifetime, which is inversely proportional to the FWHM of the absorption peak in nanodisks is longer, it does not translate to a higher absorption. At resonance the extinction cross-section of any nanopattern exceeds the geometrical area by several factors,[27] which scales differently for the complementary nanohole and nanodisk patterns. This in turn determines the effective absorption amplitude, which is higher in the case of the nanohole pattern, in spite of the shorter plasmon lifetimes. Therefore, the presence of surface plasmons breaks the symmetry of the complementary nanohole and nanodisk arrays due to their different plasmon decay rates, which suggests that maximum light absorption for respective patterns can be achieved by optimizing the geometrical area of the nanopattern such that the extinction cross-section is highest.

Geometrical Tunability. To obtain the maximum light absorption for the cavity-coupled graphene nanohole and nanodisk arrays, the optical response for different geometrical parameters (period and diameter) were simulated for a fixed Fermi energy (E_F = −1 eV) at a normal angle of incidence. For the nanohole array, a reduction in edge-to-edge distance can be achieved by either increasing the diameter for a fixed period or

DOI: 10.1021/acsnano.8b06601
ACS Nano XXXX, XXX, XXX−XXX

decreasing the period for a given diameter. By applying both strategies, we observed that the reduction in the edge-to-edge distance leads to a blue shift in the LSPR frequency, as predicted by eq 1 and shown in Figure 2a,b. In this case, the device parameters were optimized to obtain maximum absorption at λ_{res} = 8 μm.

The LSPR frequency of the nanopatterned graphene is given by[28,29,31]

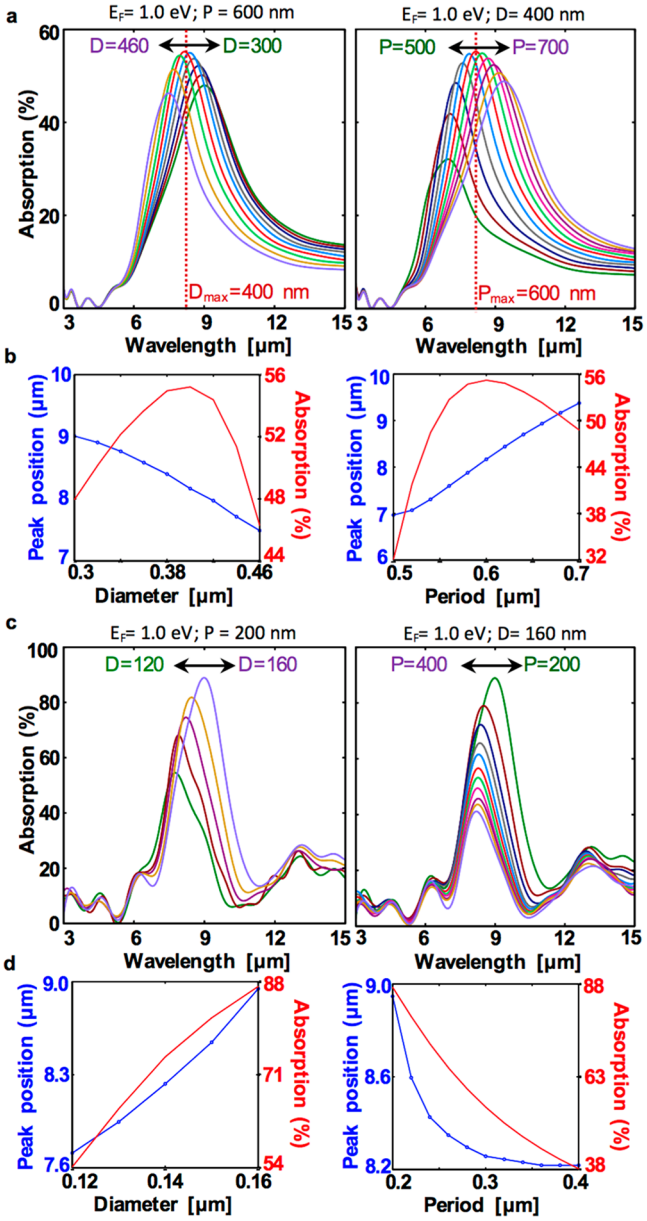

Figure 2. Geometrical tunability. (a) Light absorption of the cavity-coupled nanohole graphene with thickness L = 1.3 μm for different diameters in a constant period (P = 600 nm) (left) and different periods in a constant diameter (D = 400 nm) (right). (b) Peak position and the absorption for the graphene nanohole as a function of diameter (left) and period (right). (c) Light absorption of the cavity-coupled nanodisk graphene with thickness L= 1.5 μm for different diameters in a constant period (P = 200 nm) (left) and different periods in a constant diameter (D = 160 nm) (right). (d) Peak position and the absorption for the graphene nanodisk as a function of diameter (left) and period (right).

$$\omega_{res} = \mathcal{B}\sqrt{\frac{\mathcal{J}E_F}{d}} \quad (1)$$

where $\mathcal{B}$ is a constant value, d is the edge-to-edge distance of the nanopattern, and $\mathcal{J}$ is the eigenvalue of the self-consistent total electric potential equation. For the graphene nanodisk pattern, the increase in diameter for a constant period results in a red shift of the LSPR wavelength, as shown in Figure 2c,d and predicted by eq 1, while the decrease in the period for a constant diameter enhances the far-field and near-field coupling of the nanodisks, giving rise to a slight red shift. The amount of light absorption on the graphene nanodisk array depends on the density ratio (ρ_r), which is defined as the ratio of the graphene area to the unit cell area. The density ratio can be enhanced by increasing the diameter or decreasing the period. For a cavity thickness of L = 1.5 μm, the light absorption was found to be a continuous increasing function of the diameter and a decreasing function of period, as shown from Figure 2c,d.

Fabrication and Characterization. To validate the simulated results, absorber devices were fabricated using period and diameter values that yielded highest absorption for nanoholes and nanodisks, respectively. The nanohole and nanodisk arrays are patterned on the transferred monolayer graphene by electron beam lithography (EBL) followed by oxygen RIE. The scanning electron microscopy (SEM) images in Figure 3a show the fabricated hole and disk arrays in the

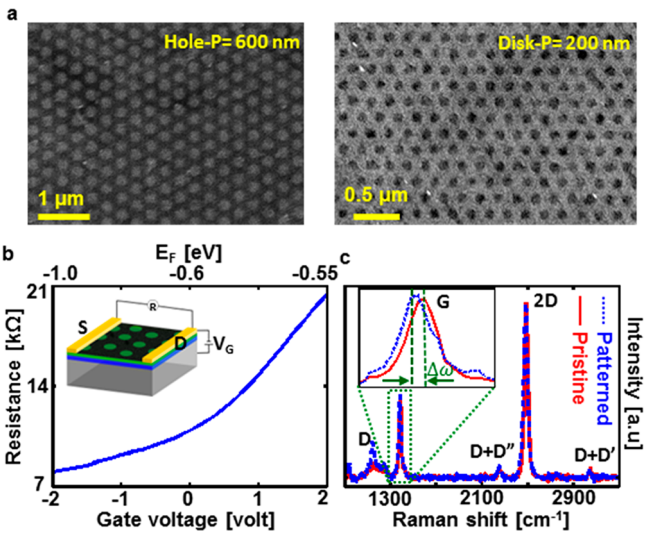

Figure 3. Fabrication and characterization. (a) SEM image of the fabricated graphene nanohole (left) and nanodisk (right). (b) Electrical resistance of the patterned graphene as a function of the gate voltage. (c) Raman spectroscopy of the pristine and patterned monolayer graphene (E_F = −0.7 eV). Electrical resistance and Raman measurements are done on the graphene hole array with P = 600 nm and D = 400 nm.

transferred graphene. A layer of semitransparent SU-8 photoresist polymer was spin-coated on the patterned graphene to form the optical cavity followed by 2 h UV exposure and 1 h baking (95 °C). A hard layer of Al_2O_3 (50 nm) is deposited on SU-8 to protect SU-8 from metal deposition, and an optically thick layer of gold (200 nm) was electron beam evaporated to form the back mirror. The Si^{2+} (100 μm) sheet used as the back gate has ~70% transmission in mid-IR range, as shown in Figure S3, and light is incident

DOI: 10.1021/acsnano.8b06601
ACS Nano XXXX, XXX, XXX−XXX

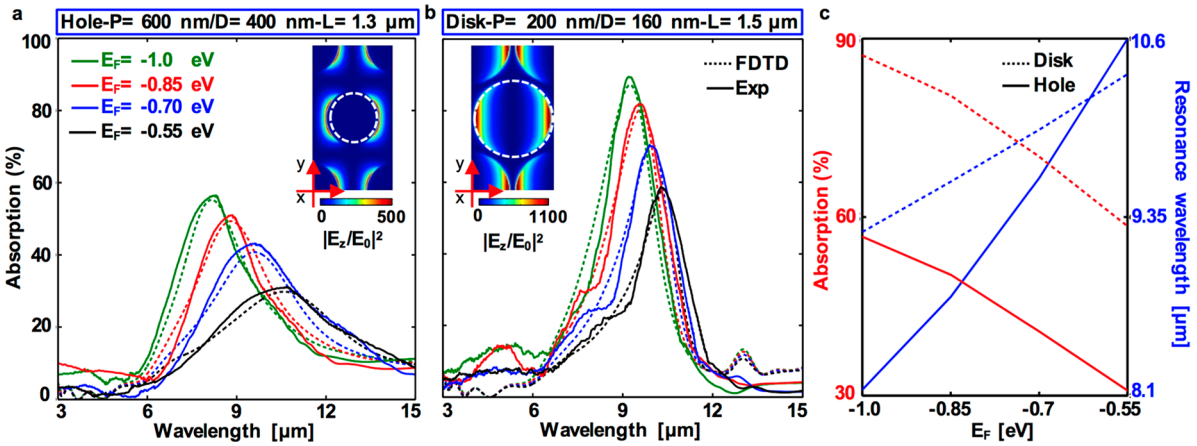

Figure 4. Experimental results of enhanced light-matter interaction. (a) Simulated and measured light absorption of the cavity-coupled graphene nanohole array with P = 600 nm, D = 400 nm, and L = 1.3 μm for different Fermi energies. (Inset) Top view of the z-component near-field profile corresponds to E_F = −1.0 eV. (b) Simulated and measured light absorption of the cavity-coupled graphene nanodisk array with P = 200 nm, D = 160 nm, and L = 1.5 μm for different Fermi energies. (Inset) Top view of the z-component near-field profile corresponds to E_F = −1.0 eV. (c) Resonance wavelength and corresponding light absorption of the cavity-coupled graphene nanodisk and nanohole arrays as a function of Fermi energy.

from the silicon side. During the transfer and fabrication process, the monolayer graphene was found to be chemically self-doped as the p-type with $E_F \sim -0.6$ eV that can be attributed to residual polymer and presence of p-type Al_2O_3 dielectric layer.[42,43] The electrostatic tunability of E_F was achieved by applying a voltage across the Al_2O_3 layer such that a negative voltage resulted in accumulation of positive charges (holes), thereby driving the system to a higher Fermi level. The Fermi energy of the nanopatterned graphene can be altered from −0.55 to −1.0 eV as shown in Figure 3bm which is associated with a decrease in channel resistance by a factor of 3. The Fermi energies of the patterned graphene corresponding to the different gate-voltages are derived *via* the measured capacitance of the gate-dielectric and, moreover, fitting to the theoretical conductivity (see the SI). An increase in the Fermi energy of graphene to $|E_F|$ = 1.0 eV is necessary to intensify the electric dipoles oscillations that allow more photons to couple to the patterned graphene edges. Our choice of high-k hard dielectric (Al_2O_3) for electrostatically doping graphene provides superior chemical stability in time over the more commonly used ion gel (see Figure S8a,b).

Raman spectroscopy was performed to confirm the quality of graphene before and after nanopatterning. As shown in Figure 3c, the characteristic 2D and G bands of graphene are visible for pristine and patterned graphene; however, a red shift ($\Delta\omega \sim 7$ cm^{-1}) in the spectrum for patterned graphene was observed, which suggests a modification in the dispersion function of the acoustic and optical phonons due to the nanopatterning[44,45] (see the SI).

Geometric and Electrostatic Tunable Absorption at Normal Incidence. The normal-angle reflection spectra of the fabricated cavity-coupled graphene nanohole and nanodisk absorbers were measured using a Bruker Vertex 80 Fourier transform infrared spectrometer (FTIR). The light reflection from the absorber stack without patterned graphene, *i.e.*, Si^{2+} (100 μm)/Al_2O_3 (15 nm)/ITO (30 nm)/SU-8 (L)/Al_2O_3 (50 nm)/gold (200 nm) was taken as the reference, and the light absorption spectrum was calculated as $A = 1 - R$. As shown in Figure 4a, the light absorption of the graphene nanohole array reaches ∼60% (at E_F = −1 eV), which is 35% higher than the previously reported maximum absorption in the 8−12 μm band.[28] Electrostatic tunability of ∼2.46 μm is observed by changing E_F from −0.55 to −1 eV. A near-perfect absorption of 90% was recorded for the nanodisk array, which is electrostatically tunable over a spectral width of ∼1.11 μm. There is in very good agreement with the simulated results. Increase in the Fermi energy to the negative values means more hole density and creation of stronger electric dipoles on the patterned graphene which results in enhanced light absorption along with a blue shift in the LSPR frequency as depicted in Figure 4c. The extraordinary near-field enhancement by factors of 500 and 1100 (inset of Figures 4a,b) for nanohole and nanodisk arrays, respectively, explain the high light−matter interaction and infrared absorption values recorded experimentally. The measured light absorption spectra of the patterned graphene without optical cavity is shown (Figure S4) along with simulated spectra ($A = 1 - T - R$) to further elucidate the excellent agreement between experiment and theory.

Angle-Dependent Infrared Absorption. To validate the operability of any absorber, it is critical to investigate its angular dependence to light. In the seminal work by Thongrattanasiri *et al.*,[27] it was analytically shown for periodically patterned graphene that under the condition of no transmission, the angular optical response to light, which depends on the polarization, is primarily determined by its mobility and extinction cross-section. Enhanced absorption would necessitate maximizing the extinction cross-section, which can be achieved by pattern optimization such that the decay rate (κ) is much higher than the radiative (κ_r) contribution ($\kappa \gg \kappa_r$). The decay rates along with the plasmon frequency ω_p determines the graphene polarizability given by

$$\alpha(\omega) = \frac{3c^3\kappa_r}{2\omega_p^2}\frac{1}{\omega_p^2 - \omega^2 - i\kappa\omega^3/\omega_p^2} \quad (2)$$

Under the assumption that the polarizabilities of monolayer graphene nanohole/nanodisk are almost independent of the angle of incidence,[29,46] the LSPR frequency is expected to not be affected by change in incident angle of light. This is confirmed by the FDTD simulations where the LSPR frequency is found to be almost independent of θ_{inc} for both

DOI: 10.1021/acsnano.8b06601
ACS Nano XXXX, XXX, XXX−XXX

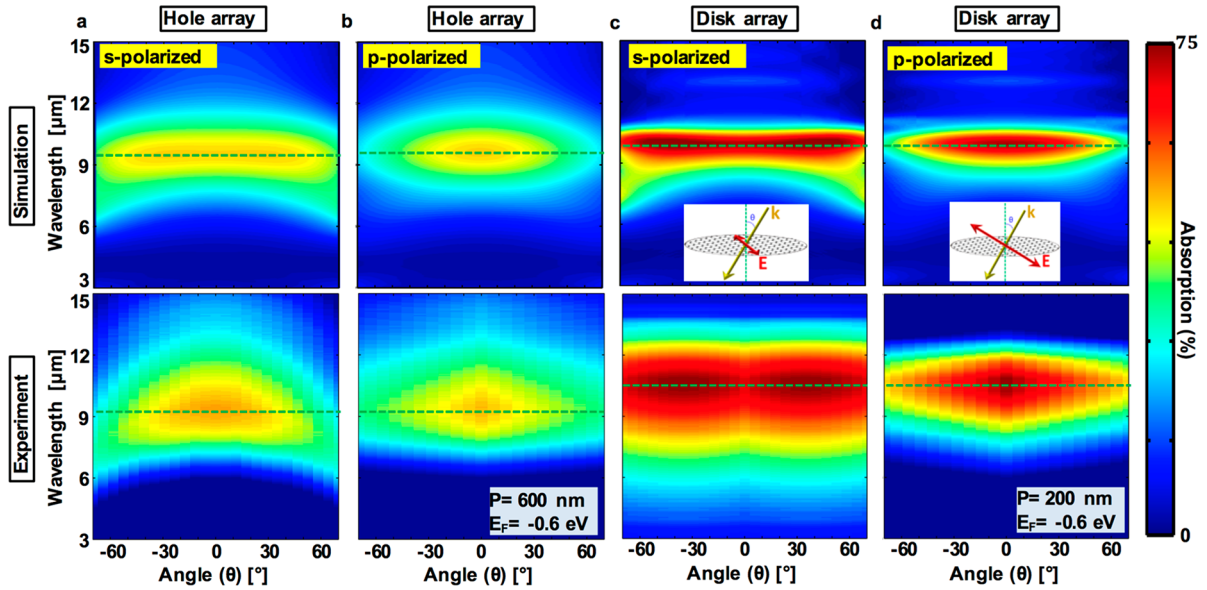

Figure 5. Angle-dependent infrared absorption. Simulation (top) and experimental (bottom) results for the angular light absorption of the cavity-coupled graphene nanohole (a, b) and nanodisk (c, d) arrays with $E_F = -0.6$ eV as a function of angle of incidence. (Inset) Schematic of the s- and p-polarized incident light. The polarized light measurements are normalized to the light intensity after the polarizer.

nanohole and nanodisk array patterned graphene with and without optical cavity (see Figures S6 and S7). At higher angles of incidence, the peak absorption of the system differs for the in-plane polarization (p-polarization) and the out-of-plane (s-polarization) light.

For p-polarized light, the absorption magnitude scales with the electric field component parallel to the surface, $E_i \cos \theta_i$ as the angle of incidence increases. In the case of s-polarized light, the LSPR frequency is almost independent of the angle of incidence for the nanohole and nanodisk array devices in the cavity coupled (Figure 5) and no-cavity (Figures S6 and S7) systems. However, the magnitude of absorption increases with angle of incidence for s-polarized light in contrast to the results obtained for p-polarized light shown in Figures S6 and S7. While the magnitude of electric field parallel to graphene surface remain unaffected for all angles of incidence (see inset of Figure 5c), the scattering cross-section increases and scales as $E_i \sin \theta_i$. This explains the enhancement in absorption as the angle of incidence increases (Figures S6 and S7). Unlike the no-cavity nanodisk array absorber, the cavity couple system exhibits an increase in absorption for $0° < \theta_i < 50°$, but for higher angles, the absorption drops (Figure 5). The temporal and spatial interference between the optical cavity and the graphene plasmonic modes modifies the angular response such that for incident angles $\theta_i > 50°$, destructive interference of the incident (E_i) and reflected electric fields (E_r) arising from the phase difference lowers the light absorption, as shown in Figure 5c. Such behavior in the angular response of cavity-coupled absorbers for s-polarized light is not uncommon and was previously shown in a VO_2-based system.[47] The FDTD predictions are well supported by experimental data (shown in Figure 5 and figures S6 and S7) acquired using an integrating sphere coupled to a FTIR.

Effect of Light Polarization on the Angular Response. While the calculations by Thongrattanasiri *et al.* were done for ideal graphene with mobility of 10000 cm/(V s), we show that it can be extended to CVD grown low mobility graphene and successfully models the FDTD and experimental results discussed below. Using eq 2 to fit the FDTD results at normal incidence, we obtain $\hbar\kappa = 3.5 \times 10^{-2}$ eV/6.9×10^{-2} eV and $\hbar\kappa_r = 1.22 \times 10^{-4}$ eV/4.5×10^{-4} eV for the graphene nanodisk/nanohole array respectively (see Figure S10), which satisfies the criteria $\kappa \gg \kappa_r$. Following that, the absorption of the patterned graphene for various incident angles can be calculated *via* the total light reflection coefficient of the cavity-coupled patterned graphene ($A = 1 - |\mathcal{R}|^2$)

$$\mathcal{R} = r_0 + \frac{r(1 \pm r_0)^2}{(1 - rr_0)} \tag{3}$$

where r_0 is the Fresnel reflection coefficient of the cavity spacer without graphene and the reflection coefficient of the patterned graphene is given by $r = \pm iS/(\alpha^{-1} - G)$[27,48] for the arrays with periods much smaller than the wavelength ($P \ll \lambda$). The lattice sum for this condition is reduced to $G = 5.52/P^3 + i(S - 2(\omega/c)^3/3)$ for hexagonal array, where S is a polarization-dependent parameter, *i.e.*, $S_s = 2\pi\omega/(cA \cos \theta_i)$, $S_p = 2\pi\omega \cos \theta_i/(cA)$ and A is the unit-cell area.[27] The calculated peak absorption as a function of incident angle for s- and p-polarized light is overlaid on the FDTD and experimentally obtained results as shown in Figure 6. Clearly a good agreement between the analytical, simulation, and experimental data is evident. Figure 6 shows the maximum absorption for different incident angles at the resonance wavelength shown by the green dash line in Figure 5. The results of the unpolarized light (Figure 6, bottom) shows that the maximum light absorption of the graphene absorber is almost independent of the incident angle for $\theta_i \leq 50°$.

CONCLUSIONS

In conclusion, we have investigated infrared absorption in an optical cavity-coupled low-carrier mobility ($\mu = 500$ cm^2/V·s) CVD-grown graphene with hexagonal array of nanoholes and nanodisks in the infrared transparent 8−12 μm band. Due to the differences in the extinction cross-section of nanohole and nanodisks for the same diameter, the plasmonic excitation on their respective edges are different, resulting in qualitatively

DOI: 10.1021/acsnano.8b06601
ACS Nano XXXX, XXX, XXX−XXX

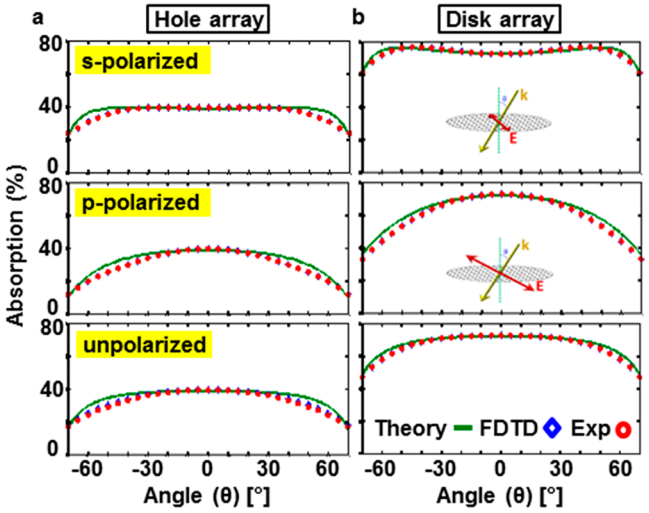

Figure 6. Angular response for the polarized and unpolarized lights. Comparison of the analytical modeling, simulation and experimental results of s-polarized (top) and p-polarized (middle) and unpolarized (down) incident light for the graphene nanohole (a) and nanodisk (b) arrays with $E_F = -0.6$ eV. The polarized light measurements are normalized to the light intensity after the polarizer.

dissimilar absorption peak profiles. A series of numerical simulations were performed to maximize infrared absorption by scanning over parameters like period and diameter for the hexagonal array of nanohole and nanodisks. The optimized devices exhibit an absorption of 60% for the nanohole array and up to 90% for nanodisk array when the Fermi level of graphene is increased to −1 eV by electrostatic p-doping. Such high absorption is attributed to strong plasmonic excitations at the patterned nanoedges where the localized electric field is amplified by factors of 500 for the nanohole and 1100 for the nanodisk arrays. For the Dirac plasmons excited by the incident light (8−12 μm), the bulk states contribute mostly to the generation of hot carriers *via* Landau damping with little contribution from the edge states. The Fermi level of the patterned graphene is tuned by applying a voltage across a 15 nm thick layer of Al_2O_3, which serves as a hard gate dielectric. The high-*k* Al_2O_3 is found to be more stable over time compared to the commonly used ionic-gel gate, which tends to chemically degrade in few days. A dynamic spectral tunability of 2.46 μm for nanoholes and 1.11 μm for nanodisks is achieved. It is to be stressed that the use of industry standard Al_2O_3 for capacitive electrostatic gating in our devices makes it a potential candidate for integration with optical design boards unlike many previously reported device architectures that are bulky due to the presence of ion-gel based components.[29,49]

In our demonstration, we showed a 1 mm^2 area absorber which is considered large area; however, we believe that the total patterned area can be increased to centimeter scale by using techniques such as nanoimprint lithography.[28,50] However, increase in the active area increases the gate leakage current resulting in inefficient electrostatic doping which is necessary to control the Fermi level for tunable absorption. Therefore, we envision an array of electrically isolated absorbers spread over centimeter scale, each with reasonable (<1 mm^2) active area, operating in tandem similar to a pixelated detector array.

Finally, by using the optimal devices with highest absorption for nanoholes and nanodisks, we show a systematic angle-dependent (0−70°) optical study in the infrared domain. Although the LSPR frequency is independent of the incident angle of light, the evolution of peak absorption for s- and p-polarized light is qualitatively dissimilar, which is attributed to the different scattering cross sections that the electric field of incident light interacts with on patterned graphene. However, the peak absorption for unpolarized light remains within 5% of its maximum up to $\theta_i \leq 50°$, which suggests that both the nanoholes and nanodisk array can be operated over a wide range of angles. These angle-dependent results provide experimental validation of the theoretical model for patterned graphene devices developed by Thongrattanasiri *et al.*[27] based on the coupled-dipole approximation. From an application point of view, the key difference between the nanohole/nanodisk arrays is the presence/absence of electrical continuity in graphene. Therefore, while the near-perfect absorption of ∼90% in the nanodisk array can be beneficial for application like wide angle optical modulators, tunable infrared camouflage, *etc.*, the nanohole array offers applicability in next-generation wide-band, wide-angle photodetectors based on electron−hole pair generation by exciting electrostatically tunable plasmons.

The photodetection scheme based on the Dirac plasmon excitation is through nonradiative plasmon decay. Upon plasmonic excitation, there are different channels for non-radiative graphene plasmon decay which depends on the wavelength of the incident light. In the electromagnetic spectral region that the optical phonons of graphene and substrate are active, they can couple to the excited plasmon and transfer the energy of surface plasmon to the atomic lattices.[28,30,34] This coupling increases the temperature of the device, thereby making bolometric infrared detection possible.[9,51−54] Alternately, one can generate hot-carriers through phonon-assisted and boundary-assisted intraband Landau damping.[9,28,30,34,55] The number of generated hot carriers, which is a function of the Fermi energy of graphene and the perimeter of the holes/disks, can be optimized to obtain enhanced electrical signal. Recent studies have attempted to utilize these approaches for detection; however, so far, the measured output responsivities have suffered due to low optical absorption.[8,9,54−61] We believe that the design for enhanced absorption presented in this study can help improve the detector performance significantly.

METHODS

Device Fabrication. A pristine graphene grown on a 25 μm thick copper foil by a CVD method was transferred to a Si^{2+} (100 μm)/Al_2O_3 (15 nm)/ITO (30 nm) substrate. The hard gate-dielectric (Al_2O_3) is grown on Si^{2+} by the atomic layer deposition (ALD). The ITO layer is sputtered on Al_2O_3 *via* an RF AJA sputtering system. The nanohole and nanodisk arrays are patterned on the transferred monolayer graphene by using EBL followed by oxygen-RIE etching and dissolving the electron resist PMMA in acetone. A layer of semitransparent SU-8 photoresist polymer as the optical cavity slab is span-coated on the patterned graphene, following by 2 h UV exposure and 1 h of baking (95 °C). A hard layer of Al_2O_3 (50 nm) is deposited on SU-8 to protect it against meta deposition, and an optically thick layer of gold (200 nm) as the back mirror is deposited on top of that.

Materials Characterization and Measurement. The theoretical simulations were performed using the FDTD method with Lumerical FDTD (Lumerical Inc.) software. The Raman spectrum of the grown graphene sheet was measured with a WITec Renishaw RM

DOI: 10.1021/acsnano.8b06601
ACS Nano XXXX, XXX, XXX−XXX

1000B Micro-Raman spectrometer with an excitation laser wavelength of 514 nm and a 50× objective lens. The real and imaginary parts of the gold dielectric function used in simulations are taken from the work of Palik.[62] The corresponding normal and non-normal incidence optical absorption measurements are performed with a integrated sphere-coupled microscope-coupled FTIR (Bruker Inc., Hyperion 1000-Vertex 80). The gate-dependent electrical conductivity is measured by using the model 2602B Keithley dual-channel system SourceMeter instrument by source-drain using two probes and the gate voltage applied using the other probes. The scanning electron microscopy was measured with Zeiss ULTRA-55 FEG SEM.

ASSOCIATED CONTENT

Supporting Information

The Supporting Information is available free of charge on the ACS Publications website at DOI: 10.1021/acsnano.8b06601.

Details of simulations, fabrication, and analysis (PDF)

AUTHOR INFORMATION

Corresponding Author

*E-mail: debashis.chanda@ucf.edu.

ORCID

Alireza Safaei: 0000-0001-9133-9680

Sayan Chandra: 0000-0003-1387-0219

Author Contributions

‡A.S. and S.C. contributed equally. A.S., S.C., and DC. conceived the idea. A.S. designed and performed the experiments. S.C. provided technical assistance. A.S., S.C., and D.C. analyzed and simulated the data. M.L. and D.C. contributed materials/analysis tools. A.S., S.C., and D.C. cowrote the paper.

Notes

The authors declare no competing financial interest.

ACKNOWLEDGMENTS

This work at the University of Central Florida was supported by DARPA under the WIRED program (Grant No. HR0011-16-1-0003).

REFERENCES

(1) Bonaccorso, F.; Sun, Z.; Hasan, T.; Ferrari, A. C. Graphene Photonics and Optoelectronics. *Nat. Photonics* **2010**, *4*, 611−622.

(2) Falkovsky, L. A. Optical Properties of Doped Graphene Layers. *J. Exp. Theor. Phys.* **2008**, *106*, 575−580.

(3) Falkovsky, L. A.; Pershoguba, S. S. Optical Far-Infrared Properties of a Graphene Monolayer and Multilayer. *Phys. Rev. B: Condens. Matter Mater. Phys.* **2007**, *76*, No. 153410.

(4) Falkovsky, L. A.; Varlamov, A. A. Space-Time Dispersion of Graphene Conductivity. *Eur. Phys. J. B* **2007**, *56*, 281−284.

(5) Singh, V.; Joung, D.; Zhai, L.; Das, S.; Khondaker, S. I.; Seal, S. Graphene Based Materials: Past, Present and Future. *Prog. Mater. Sci.* **2011**, *56*, 1178−1271.

(6) Hemmatiyan, S.; Polini, M.; Abanov, A.; MacDonald, A. H.; Sinova, J. Stable Path to Ferromagnetic Hydrogenated Graphene Growth. *Phys. Rev. B: Condens. Matter Mater. Phys.* **2014**, *90*, No. 035433.

(7) Schwierz, F. Graphene Transistors. *Nat. Nanotechnol.* **2010**, *5*, 487−496.

(8) Sun, Z.; Chang, H. Graphene and Graphene-Like Two-Dimensional Materials in Photodetection: Mechanisms and Methodology. *ACS Nano* **2014**, *8*, 4133−4156.

(9) Freitag, M.; Low, T.; Zhu, W.; Yan, H.; Xia, F.; Avouris, P. Photocurrent in Graphene Harnessed by Tunable Intrinsic Plasmons. *Nat. Commun.* **2013**, *4*, 1951.

(10) Yao, Y.; Shankar, R.; Kats, M. A.; Song, Y.; Kong, J.; Loncar, M.; Capasso, F. Electrically Tunable Metasurface Perfect Absorbers for Ultrathin Mid-Infrared Optical Modulators. *Nano Lett.* **2014**, *14*, 6526−6532.

(11) Sun, Z.; Hasan, T.; Torrisi, F.; Popa, D.; Privitera, G.; Wang, F.; Bonaccorso, F.; Basko, D. M.; Ferrari, A. C. Graphene Mode-Locked Ultrafast Laser. *ACS Nano* **2010**, *4*, 803−810.

(12) Lu, Y.; Goldsmith, B. R.; Kybert, N. J.; Johnson, A. T. C. DNA-Decorated Graphene Chemical Sensors. *Appl. Phys. Lett.* **2010**, *97*, 083107.

(13) Yavari, F.; Koratkar, N. Graphene-Based Chemical Sensors. *J. Phys. Chem. Lett.* **2012**, *3*, 1746−1753.

(14) Singh, E.; Meyyappan, M.; Nalwa, H. S. Flexible Graphene-Based Wearable Gas and Chemical Sensors. *ACS Appl. Mater. Interfaces* **2017**, *9*, 34544−34586.

(15) Nair, R. R.; Blake, P.; Grigorenko, A. N.; Novoselov, K. S.; Booth, T. J.; Stauber, T.; Peres, N. M.; Geim, A. K. Fine Structure Constant Defines Visual Transparency of Graphene. *Science* **2008**, *320*, 1308.

(16) Yan, H.; Xia, F.; Zhu, W.; Freitag, M.; Dimitrakopoulos, C.; Bol, A. A.; Tulevski, G.; Avouris, P. Infrared Spectroscopy of Wafer-Scale Graphene. *ACS Nano* **2011**, *5*, 9854−9860.

(17) Gan, X.; Shiue, R. J.; Gao, Y.; Mak, K. F.; Yao, X.; Li, L.; Szep, A.; Walker, D., Jr.; Hone, J.; Heinz, T. F.; Englund, D. High-Contrast Electrooptic Modulation of a Photonic Crystal Nanocavity by Electrical Gating of Graphene. *Nano Lett.* **2013**, *13*, 691−696.

(18) Otsuji, T.; Popov, V.; Ryzhii, V. Active Graphene Plasmonics for Terahertz Device Applications. *J. Phys. D: Appl. Phys.* **2014**, *47*, 094006.

(19) Zhang, Y.; Feng, Y.; Zhu, B.; Zhao, J.; Jiang, T. Graphene Based Tunable Metamaterial Absorber and Polarization Modulation in Terahertz Frequency. *Opt. Express* **2014**, *22*, 22743−22752.

(20) Majumdar, A.; Kim, J.; Vuckovic, J.; Wang, F. Graphene for Tunable Nanophotonic Resonators. *IEEE J. Sel. Top. Quantum Electron.* **2014**, *20*, 4600204.

(21) Li, J.; Yu, P.; Cheng, H.; Liu, W.; Li, Z.; Xie, B.; Chen, S.; Tian, J. Optical Polarization Encoding Using Graphene-Loaded Plasmonic Metasurfaces. *Adv. Opt. Mater.* **2016**, *4*, 91−98.

(22) Kim, S.; Jang, M. S.; Brar, V. W.; Mauser, K. W.; Kim, L.; Atwater, H. A. Electronically Tunable Perfect Absorption in Graphene. *Nano Lett.* **2018**, *18*, 971−979.

(23) Brar, V. W.; Jang, M. S.; Sherrott, M.; Lopez, J. J.; Atwater, H. A. Highly Confined Tunable Mid-Infrared Plasmonics in Graphene Nanoresonators. *Nano Lett.* **2013**, *13*, 2541−2547.

(24) Ju, L.; Geng, B.; Horng, J.; Girit, C.; Martin, M.; Hao, Z.; Bechtel, H. A.; Liang, X.; Zettl, A.; Shen, Y. R.; Wang, F. Graphene Plasmonics for Tunable Terahertz Metamaterials. *Nat. Nanotechnol.* **2011**, *6*, 630−634.

(25) Furchi, M.; Urich, A.; Pospischil, A.; Lilley, G.; Unterrainer, K.; Detz, H.; Klang, P.; Andrews, A. M.; Schrenk, W.; Strasser, G.; Mueller, T. Microcavity-Integrated Graphene Photodetector. *Nano Lett.* **2012**, *12*, 2773−2777.

(26) Alaee, R.; Farhat, M.; Rockstuhl, C.; Lederer, F. A Perfect Absorber Made of a Graphene Micro-Ribbon Metamaterial. *Opt. Express* **2012**, *20*, 28017−28024.

(27) Thongrattanasiri, S.; Koppens, F. H.; Garcia de Abajo, F. J. Complete Optical absorption in Periodically Patterned Graphene. *Phys. Rev. Lett.* **2012**, *108*, 047401.

(28) Safaei, A.; Chandra, S.; Vázquez-Guardado, A.; Calderon, J.; Franklin, D.; Tetard, L.; Zhai, L.; Leuenberger, M. N.; Chanda, D. Dynamically Tunable Extraordinary Light Absorption in Monolayer Graphene. *Phys. Rev. B: Condens. Matter Mater. Phys.* **2017**, *96*, 165431.

(29) Fang, Z.; Thongrattanasiri, S.; Schlather, A.; Liu, Z.; Ma, L.; Wang, Y.; Ajayan, P. M.; Nordlander, P.; Halas, N. J.; Garcia de Abajo, F. J. Gated Tunability and Hybridization of Localized Plasmons in Nanostructured Graphene. *ACS Nano* **2013**, *7*, 2388−2395.

DOI: 10.1021/acsnano.8b06601
ACS Nano XXXX, XXX, XXX−XXX

(30) Paudel, H. P.; Safaei, A.; Leuenberger, M. N.. Nanoplasmonics in Metallic Nanostructures and Dirac Systems. In *Nanoplasmonics - Fundamentals and Applications*; Barbillon, D. G., Ed.; InTech, 2017; Chapter 3.
(31) Gao, W.; Shu, J.; Qiu, C.; Xu, Q. Excitation of Plasmonic Waves in Graphene by Guided-Mode Resonances. *ACS Nano* **2012**, *6*, 7806−7813.
(32) Cheng, H.; Chen, S.; Yu, P.; Liu, W.; Li, Z.; Li, J.; Xie, B.; Tian, J. Dynamically Tunable Broadband Infrared Anomalous Refraction Based on Graphene Metasurfaces. *Adv. Opt. Mater.* **2015**, *3*, 1744−1749.
(33) Cheng, H.; Chen, S.; Yu, P.; Duan, X.; Xie, B.; Tian, J. Dynamically Tunable Plasmonically Induced Transparency in Periodically Patterned Graphene Nanostrips. *Appl. Phys. Lett.* **2013**, *103*, 203112.
(34) Yan, H. G.; Low, T.; Zhu, W. J.; Wu, Y. Q.; Freitag, M.; Li, X. S.; Guinea, F.; Avouris, P.; Xia, F. N. Damping Pathways of Mid-Infrared Plasmons in Graphene Nanostructures. *Nat. Photonics* **2013**, *7*, 394−399.
(35) Fei, Z.; Goldflam, M. D.; Wu, J. S.; Dai, S.; Wagner, M.; McLeod, A. S.; Liu, M. K.; Post, K. W.; Zhu, S.; Janssen, G. C.; Fogler, M. M.; Basov, D. N. Edge and Surface Plasmons in Graphene Nanoribbons. *Nano Lett.* **2015**, *15*, 8271−8276.
(36) Brown, A. M.; Sundararaman, R.; Narang, P.; Goddard, W. A., 3rd; Atwater, H. A. Nonradiative Plasmon Decay and Hot Carrier Dynamics: Effects of Phonons, Surfaces, and Geometry. *ACS Nano* **2016**, *10*, 957−966.
(37) Sundararaman, R.; Narang, P.; Jermyn, A. S.; Goddard, W. A.; Atwater, H. A. Theoretical Predictions for Hot-Carrier Generation from Surface Plasmon Decay. *Nat. Commun.* **2014**, *5*, 5788.
(38) Safaei, A.; Vázquez-Guardado, A.; Franklin, D.; Leuenberger, M. N.; Chanda, D. High-Efficiency Broadband Mid-Infrared Flat Lens. *Adv. Opt. Mater.* **2018**, *6*, 1800216.
(39) Vazquez-Guardado, A.; Safaei, A.; Modak, S.; Franklin, D.; Chanda, D. Hybrid Coupling Mechanism in a System Supporting High Order Diffraction, Plasmonic, and Cavity Resonances. *Phys. Rev. Lett.* **2014**, *113*, 263902.
(40) Chandra, S.; Franklin, D.; Cozart, J.; Safaei, A.; Chanda, D. Adaptive Multispectral Infrared Camouflage. *ACS Photonics* **2018**, *5*, 4513−4519.
(41) Safaei, A.; Modak, S.; Vasquez-Gaurdado, A.; Franklin, D.; Chanda, D. Cavity-Induced Hybrid Plasmon Excitation for Perfect Infrared Absorption. *Opt. Lett.* **2018**, *43*, 230001−230004.
(42) Shin, S.; Kim, S.; Kim, T.; Du, H.; Kim, K. S.; Cho, S.; Seo, S. Graphene Transfer with Self-Doping by Amorphous Thermoplastic Resins. *Carbon* **2017**, *111*, 215−220.
(43) Deng, C.; Lin, W.; Agnus, G.; Dragoe, D.; Pierucci, D.; Ouerghi, A.; Eimer, S.; Barisic, I.; Ravelosona, D.; Chappert, C.; Zhao, W. Reversible Charge-Transfer Doping in Graphene due to Reaction with Polymer Residues. *J. Phys. Chem. C* **2014**, *118*, 13890−13897.
(44) Maultzsch, J.; Reich, S.; Thomsen, C.; Requardt, H.; Ordejon, P. Phonon Dispersion in Graphite. *Phys. Rev. Lett.* **2004**, *92*, 075501.
(45) Qian, J.; Allen, M. J.; Yang, Y.; Dutta, M.; Stroscio, M. A. Quantized Long-Wavelength Optical Phonon Modes in Graphene Nanoribbon in the Elastic Continuum Model. *Superlattices Microstruct.* **2009**, *46*, 881−888.
(46) Maier, S. A. *Plasmonics: Fundamentals and Applications*; Springer, 2007.
(47) Kocer, H.; Butun, S.; Palacios, E.; Liu, Z.; Tongay, S.; Fu, D.; Wang, K.; Wu, J.; Aydin, K. Intensity Tunable Infrared Broadband Absorbers Based on VO_2 Phase Transition Using Planar Layered Thin Films. *Sci. Rep.* **2015**, *5*, 13384.
(48) García de Abajo, F. J. Colloquium: Light Scattering by Particle and Hole Arrays. *Rev. Mod. Phys.* **2007**, *79*, 1267−1290.
(49) Cho, J. H.; Lee, J.; Xia, Y.; Kim, B.; He, Y.; Renn, M. J.; Lodge, T. P.; Frisbie, C. D. Printable Ion-Gel Gate Dielectrics for Low-Voltage Polymer Thin-Film Transistors on Plastic. *Nat. Mater.* **2008**, *7*, 900−906.
(50) Liang, X.; Jung, Y. S.; Wu, S.; Ismach, A.; Olynick, D. L.; Cabrini, S.; Bokor, J. Formation of Bandgap and Subbands in Graphene Nanomeshes with Sub-10 nm Ribbon Width Fabricated *via* Nanoimprint Lithography. *Nano Lett.* **2010**, *10*, 2454−2460.
(51) Ju, L.; Geng, B.; Horng, J.; Girit, C.; Martin, M.; Hao, Z.; Bechtel, H. A.; Liang, X.; Zettl, A.; Shen, Y. R.; Wang, F. Graphene Plasmonics for Tunable Terahertz Metamaterials. *Nat. Nanotechnol.* **2011**, *6*, 630−634.
(52) Chanda, D.; Safaei, A.; N. Leuenberger, M. Optical Detector Device with Patterned Graphene Layer and Related Methods. US Patent Appl. 15/782,948, 2018.
(53) Chanda, D.; Modak, S.; Lee, J.; Safaei, A. Optical Frequency-Selective Absorber-Based Infrared Detector, Methods, and Applications. US Patent Appl. 15/538,746, 2018.
(54) Freitag, M.; Low, T.; Martin-Moreno, L.; Zhu, W.; Guinea, F.; Avouris, P. Substrate-Sensitive Mid-Infrared Photoresponse in Graphene. *ACS Nano* **2014**, *8*, 8350−8356.
(55) Song, J. C.; Rudner, M. S.; Marcus, C. M.; Levitov, L. S. Hot Carrier Transport and Photocurrent Response in Graphene. *Nano Lett.* **2011**, *11*, 4688−4692.
(56) Sun, D.; Aivazian, G.; Jones, A. M.; Ross, J. S.; Yao, W.; Cobden, D.; Xu, X. Ultrafast Hot-Carrier-Dominated Photocurrent in Graphene. *Nat. Nanotechnol.* **2012**, *7*, 114−118.
(57) Guo, Q.; Yu, R.; Li, C.; Yuan, S.; Deng, B.; Garcia de Abajo, F. J.; Xia, F. Efficient Electrical Detection of Mid-Infrared Graphene Plasmons at Room Temperature. *Nat. Mater.* **2018**, *17*, 986−992.
(58) Cai, X.; Sushkov, A. B.; Suess, R. J.; Jadidi, M. M.; Jenkins, G. S.; Nyakiti, L. O.; Myers-Ward, R. L.; Li, S.; Yan, J.; Gaskill, D. K.; Murphy, T. E.; Drew, H. D.; Fuhrer, M. S. Sensitive Room-Temperature Terahertz Detection *via* the Photothermoelectric Effect in Graphene. *Nat. Nanotechnol.* **2014**, *9*, 814−819.
(59) Xu, X.; Gabor, N. M.; Alden, J. S.; van der Zande, A. M.; McEuen, P. L. Photo-Thermoelectric Effect at a Graphene Interface Junction. *Nano Lett.* **2010**, *10*, 562−566.
(60) Liu, C. H.; Chang, Y. C.; Norris, T. B.; Zhong, Z. H. Graphene Photodetectors with Ultra-Broadband and High Responsivity at Room Temperature. *Nat. Nanotechnol.* **2014**, *9*, 273−278.
(61) Mueller, T.; Xia, F. N. A.; Avouris, P. Graphene Photodetectors for High-Speed Optical Communications. *Nat. Photonics* **2010**, *4*, 297−301.
(62) Palik, E. D. *Handbook of Optical-Constants*; Academic, 1984.

DOI: 10.1021/acsnano.8b06601
ACS Nano XXXX, XXX, XXX−XXX